Electronic Supplementary Material (ESI) for ChemComm.

Supporting Information

Selenium vacancy triggered atomic disordering of $Co_{0.85}Se$ nanoparticles towards highly-active electrocatalyst for water oxidation

Jiahao Zhang,[a] Qiucheng Xu,[a] Yanjie Hu,[a] Hao Jiang,[a] and Chunzhong Li[a]*

[a] Key Laboratory for Ultrafine Materials of Ministry of Education, Shanghai Engineering Research Center of Hierarchical Nanomaterials, School of Materials Science and Engineering, East China University of Science and Technology, Shanghai 200237, China

* E-mail: jianghao@ecust.edu.cn (Prof. H. Jiang)

Part I: Experimental

Synthesis of the V_{Se}-engineered $Co_{0.85}Se$ nanoparticles

Co foam (CF, 5 mm × 7 mm × 0.3 mm) was firstly pretreated by sonicating in 3 M HCl for 20 min to remove surface oxide layer and impurities. The $Co_{0.85}Se$ nanoparticles were simply synthesized through a solid-phase melting strategy in a glovebox filled with Ar gas. In detail, a piece of CF was placed in the bottom of a flask, and 9 mg Se powder was added to well-wrap the surface of CF. Subsequently, the device was heated at 250 °C for a certain time. After natural cooling down to room temperature, the resulting samples were washed with CS_2, absolute ethanol and deionized water for three times, respectively. Finally, the $Co_{0.85}Se$ samples were obtained after dried at 60 °C overnight in a vacuum oven. The as-prepared $Co_{0.85}Se$ samples were denoted as $Co_{0.85}Se$-Time (unit: min). The mass loading of the $Co_{0.85}Se$ nanoparticles on CF is about 10.5 mg cm^{-2}.

Structured characterization

The powder X-ray diffraction (XRD) patterns were carried out by a Rigaku D/Max 2550 diffractometer (Cu Ka radiation) at a scan rate of 1 ° min^{-1}. X-ray photoelectron spectroscopy (XPS) spectra were recorded by an ESCALAB 250Xi X-ray photoelectron spectrometer (Al Kα X-ray source) at a pass energy of 40 eV. The inductively coupled plasma mass spectrometry (ICP-MS) was performed by an Agilent 7700 spectrometer. The microstructure of the as-obtained samples was observed by field emission scanning electron microscopy (FESEM, Hitachi, S-4800, 15 kV) and transmission electron microscopy (TEM, JEOL, JEM-2100F) with an X-ray energy dispersive spectrometer (EDS) at an accelerating voltage of 200 kV.

Electrochemical Measurements

All electrochemical measurements were carried out by a CHI660E electrochemical workstation (CH Instruments, Inc., Shanghai, China) with a standard three-electrode system in 1 M KOH. The electrocatalysts supported on CF were directly applied as working electrode, while a saturated Ag/AgCl electrode and a graphite electrode were applied as reference electrode and counter electrode, respectively. For RuO_2, 5 mg powder, 0.4 mL distilled water,

0.52 mL ethanol and 80 μL Nafion solution (5 wt%) were adequately sonicated and then drop-coated onto CF with a mass loading of 3 mg cm-2. The OER activity of RuO_2 is optimal via the balance between true active component exposure and mass loading. The measured potentials were calibrated to a reversible hydrogen electrode (RHE) according to the following equation:

$$E_{RHE} = E_{Ag/AgCl} + 0.1976 + 0.0591 \times pH$$

The OER polarization curves were measured by linear sweep voltammetry (LSV) technique with a scan rate of 5 mV s^{-1}. The durable stability of the optimal sample was recorded by chronopotentiometry (CP) under multiple current densities of 10, 20, 50, 100 and 150 mA cm^{-2}. The aforementioned electrochemical data were compensated with a 95% *iR* correction. Turnover frequency (TOF) values were estimated from the following equation:

$$TOF = (J \times A) / (4 \times n \times F)$$

Where J is the current density, A is the geometric surface area, n is the mole number of active metal sites, and F is the Faraday constant (96485 C mol^{-1}). Electrochemically active surface area (ECSA) was calculated based on the following equation:

$$ECSA = C_{DL}/C_S$$

Where C_{DL} is double layer capacitance, and C_S is specific capacitance. The C_{DL} was obtained through multi-rate cycle-voltage (CV) in non-faradic potential range. The C_S is 40 μF cm^{-2} according to the previous literature.[S1] The apparent activation energy (E_a) was estimated from the Arrhenius equation:

$$\ln(j) = - E_a/RT + C$$

Where j is the current density, R is the gas constant (8.3145 J mol^{-1} K^{-1}), and T is the Kelvin temperature.[S2] Electrochemical impedance spectroscopy (EIS) in a frequency range from 0.01 Hz to 100 kHz was performed by an Autolab PGSTAT302N electrochemical workstation at 1.48 V. Tafel slopes (b) were calculated by fitting the Tafel plots:

$$\eta = b\log(j) + a$$

Where η is the overpotential, and j is the corresponding current density.

Part II: Supporting Figures

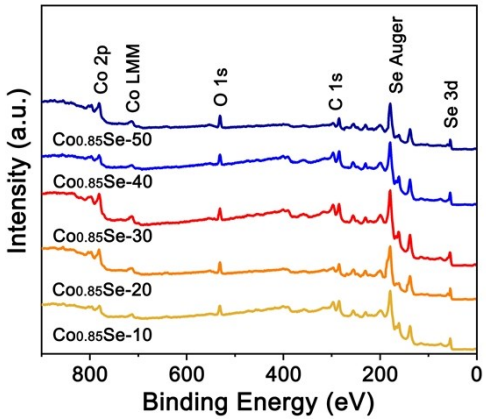

Fig. S1 Full XPS spectra of the V_{Se}-engineered $Co_{0.85}Se$ samples.

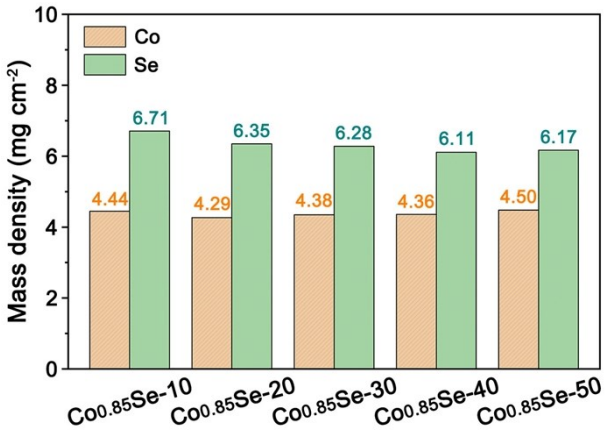

Fig. S2 Mass densities of Co and Se in the V_{Se}-engineered $Co_{0.85}Se$ samples. The mass densities of Co element (m_{Co}) are estimated from the following equation:

$$m_{Co} = m_{Se} \times R_{Co/Se} \times M_{Co}/M_{Se}$$

Where m_{Se} is the Se content based on ICP-MS, $R_{Co/Se}$ is the ratio of Co to Se according to XPS, and M_{Co} and M_{Se} are the molecular mass of Co and Se, respectively.

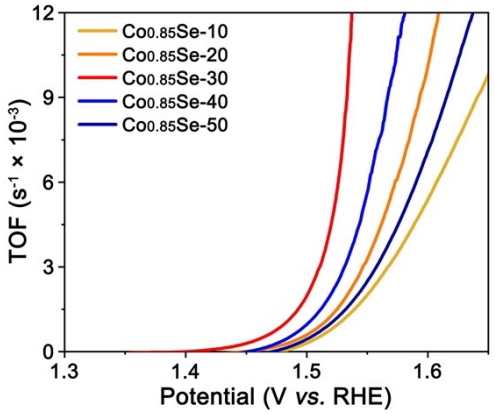

Fig. S3 TOF curves of the V_{Se}-engineered $Co_{0.85}Se$ samples.

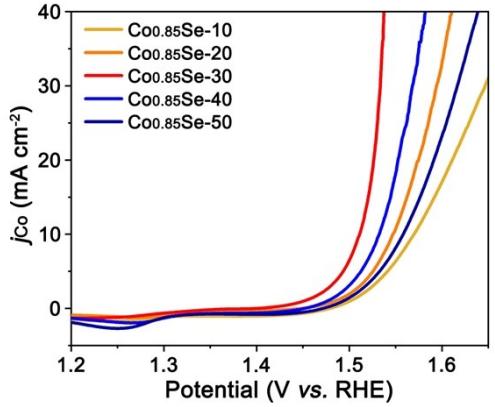

Fig. S4 Mass-normalized OER polarization curves of the V_{Se}-engineered $Co_{0.85}Se$ samples.

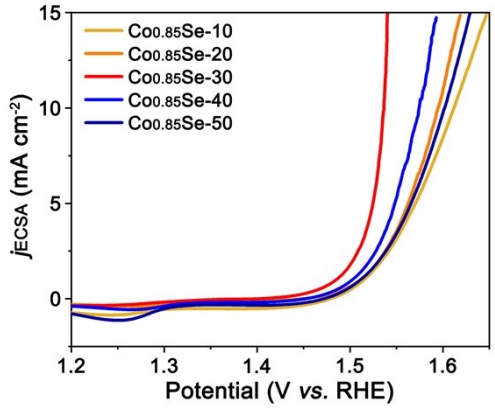

Fig. S5 ECSA-normalized OER polarization curves of the V_{Se}-engineered $Co_{0.85}Se$ samples.

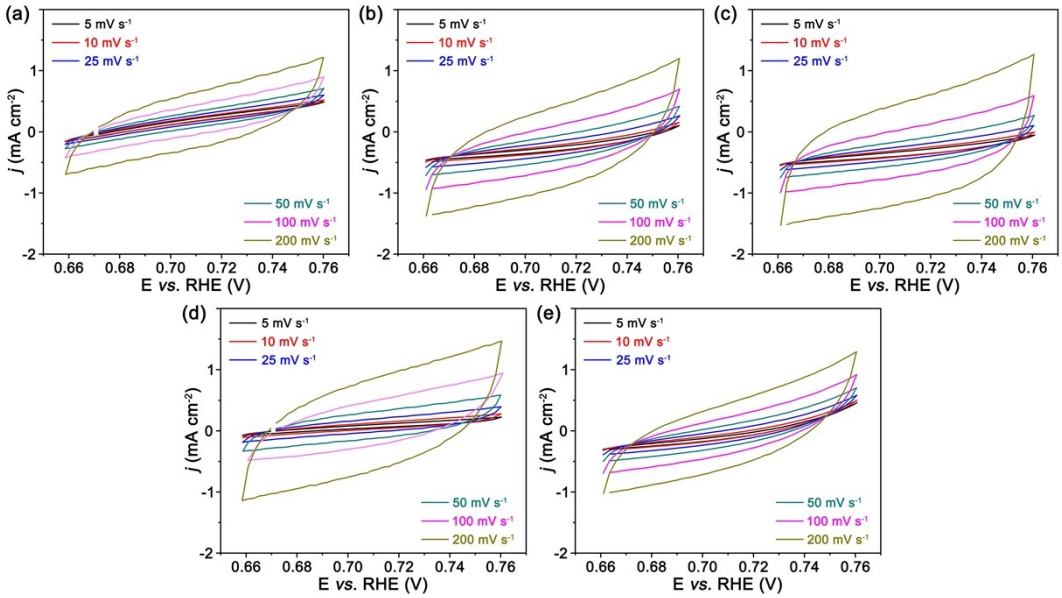

Fig. S6 Cyclic voltammograms curves of (a) $Co_{0.85}Se$-10, (b) $Co_{0.85}Se$-20, (c) $Co_{0.85}Se$-30, (d) $Co_{0.85}Se$-40 and (e) $Co_{0.85}Se$-50 in non-faradic potential range at different sweep rates.

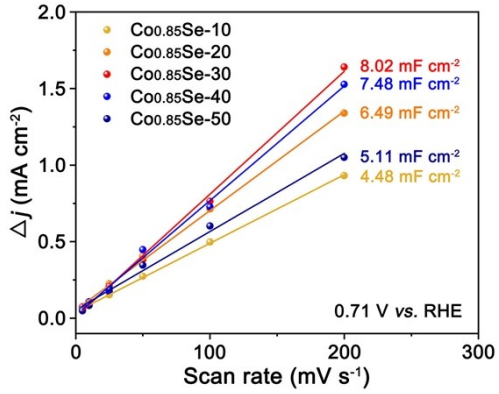

Fig. S7 C_{DL} of the V_{Se}-engineered $Co_{0.85}Se$ samples.

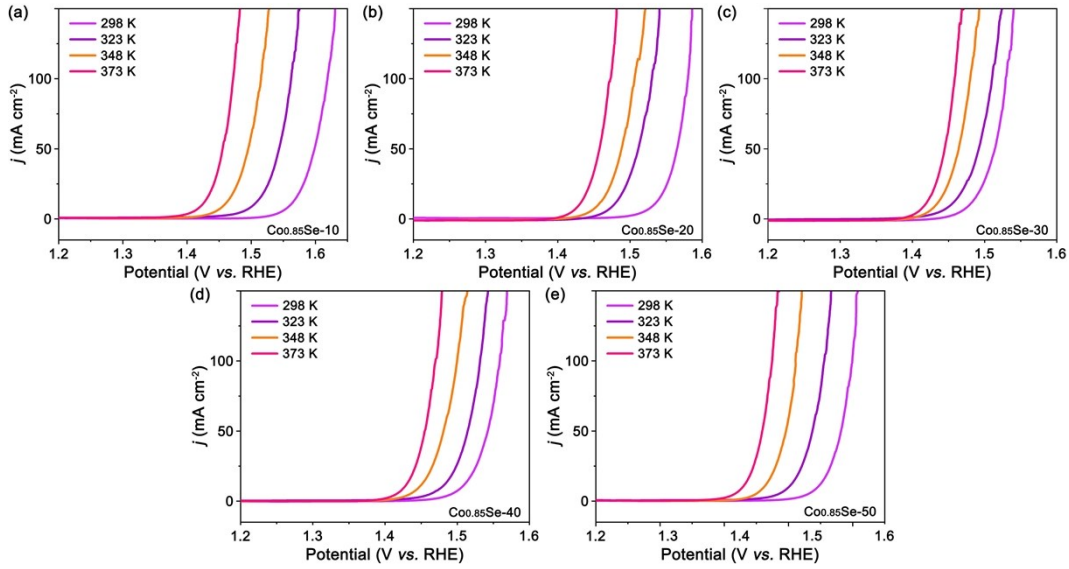

Fig. S8 OER polarization curves of (a) $Co_{0.85}Se$-10, (b) $Co_{0.85}Se$-20, (c) $Co_{0.85}Se$-30, (d) $Co_{0.85}Se$-40 and (e) $Co_{0.85}Se$-50 in 1 M KOH at 25, 50, 75, and 100 ℃, respectively.

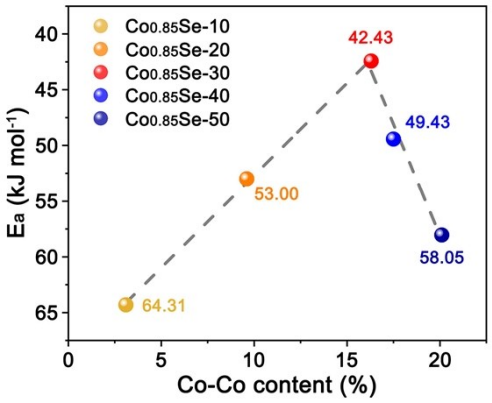

Fig. S9 Volcano-shaped correlation for E_a values of the V_{Se}-engineered $Co_{0.85}Se$ samples depends on Co-Co content.

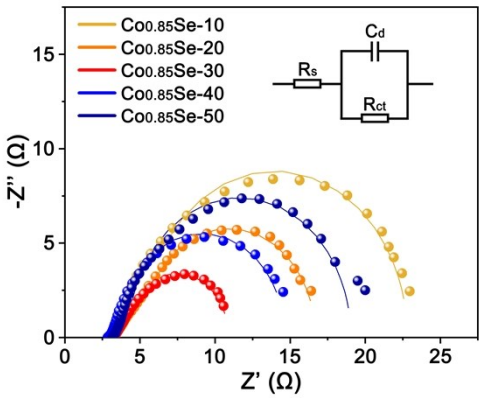

Fig. S10 Nyquist plots of the V_{Se}-engineered $Co_{0.85}Se$ samples.

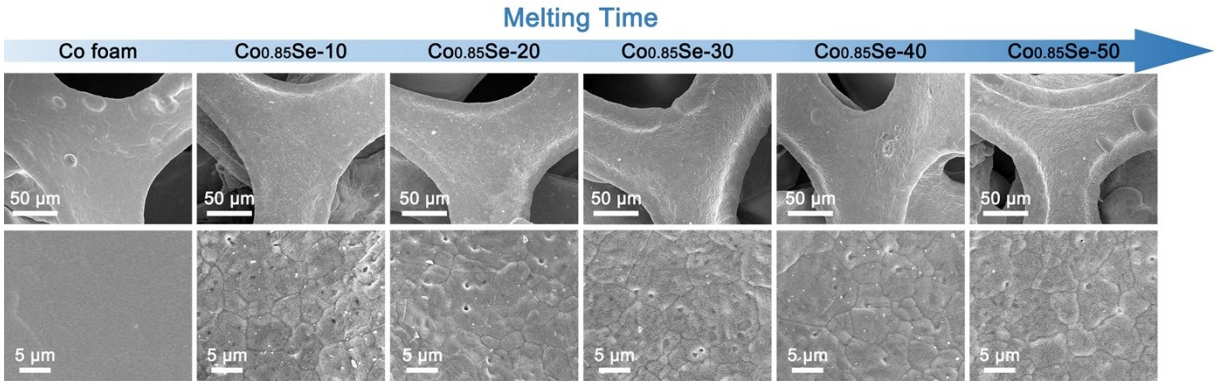

Fig. S11 SEM images of the bare CF and V_{Se}-engineered $Co_{0.85}Se$ samples.

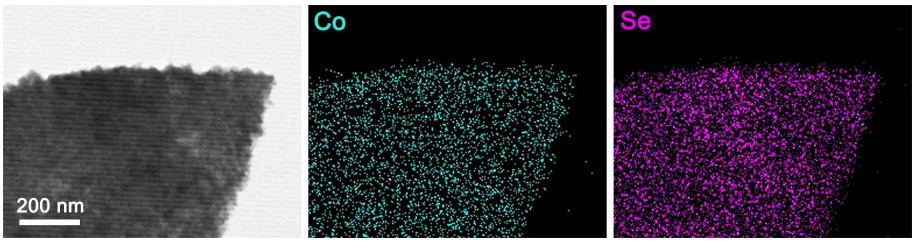

Fig. S12 TEM-EDS mapping of the $Co_{0.85}Se$-30 sample.

Part III: Supporting Tables

Table S1 Comparison for OER performance of cobalt-selenide-based electrocatalysts.

Electrocatalysts	Electrolyte	η @ 10 mA cm^{-2}	Tafel slope	Ref.
ZIF-$Co_{0.85}Se$	1 M KOH	360 mV	62 mV dec^{-1}	S3
$Co_{0.85}Se$@NC	1 M KOH	320 mV	75 mV dec^{-1}	S4
Ti@$Co_{0.85}Se$	1 M PBS	500 mV	153 mV dec^{-1}	S5
$Co_{0.85}Se$@CNFs	0.1 M KOH	350 mV	61 mV dec^{-1}	S6
$Co_{0.85}Se$/HPG	0.1 M KOH	385 mV	61.7 mV dec^{-1}	S7
$Co_{0.85}Se$ spheres	1 M KOH	290 mV	81 mV dec^{-1}	S8
Vacancy-Rich $CoSe_2$	0.1 M KOH	320 mV	44 mV dec^{-1}	S9
$Zn_{0.1}Co_{0.9}Se_2$	1 M KOH	340 mV	43.2 mV dec^{-1}	S10
o-$CoSe_2$-O UNs	1 M KOH	251 mV	73 mV dec^{-1}	S11
Cu-14-Co_3Se_4/GC	0.1 M KOH	280 mV	111 mV dec^{-1}	S12
$CoSe_{1.26}P_{1.42}$	1 M KOH	255 mV	87 mV dec^{-1}	S13
$CoSe_2$ UNM_{vac}	1 M KOH	284 mV	46.3 mV dec^{-1}	S14
$Co_{0.85}Se$-30	**1 M KOH**	**243 mV**	**45.5 mV dec^{-1}**	**This work**

Table S2 Composition of the V_{Se}-engineered $Co_{0.85}Se$ samples estimated from the XPS measurements.

Samples	$Co_{0.85}Se$-10	$Co_{0.85}Se$-20	$Co_{0.85}Se$-30	$Co_{0.85}Se$-40	$Co_{0.85}Se$-50
X in $Co_{0.85}Se_{1-X}$	0.043	0.057	0.085	0.110	0.127

Table S3 Geometric values of the electronic elements extracted from the electrical equivalent circuit model.

Electrocatalysts	R_s (Ω)	R_{ct} (Ω)	C_{dl} (F)
$Co_{0.85}Se$-10	4.180	18.62	0.1076
$Co_{0.85}Se$-20	4.128	12.56	0.1536
$Co_{0.85}Se$-30	3.503	8.185	0.1583
$Co_{0.85}Se$-40	3.631	11.01	0.1321
$Co_{0.85}Se$-50	4.228	14.81	0.1159

R_s is related to the series resistance. R_{ct} denotes the charge transfer resistance. C_{dl} is the constant phase angle element, representing the double layer capacitance.

References

S1. C. C. L. McCrory, S. Jung, I. M. Ferrer, S. M. Chatman, J. C. Peters and T. F. Jaramillo, *J. Am. Chem. Soc.*, 2015, **137**, 4347-4357.

S2. M. Wang, C. Dong, Y. Huang, Y. Li and S. Shen, *Small*, 2018, **14**, 1801756.

S3. S. Li, S. Peng, L. Huang, X. Cui, A. M. Al-Enizi and G. Zheng, *ACS Appl. Mater. Interfaces*, 2016, **8**, 20534-20539.

S4. T. Meng, J. Qin, S. Wang, D. Zhao, B. Mao and M. Cao, *J. Mater. Chem. A*, 2017, **5**, 7001-7014.

S5. J. Zhang, H. Su, H. Wang, Z. Xue, B. Zhang, X. Wei, X. Li, S. Hirano and J. Chen, *Nano Energy*, 2017, **39**, 321-327.

S6. L. Gui, Z. Huang, D. Ai, B. He, W. Zhou, J. Sun, J. Xu, Q. Wang and L. Zhao, *Chem. Eur. J.*, 2019, **25**, 1-8.

S7. Q. Zhong, W. Xia, B. Liu, C. Xu and N. Li, *Int. J. Hydrogen Energy*, 2019, **44**, 10182-10189.

S8. N. Hussain, F. Wu, L. Xu and Y. Qian, *Nano Res.*, 2019, **12**, 2941-2946.

S9. Y. Liu, H. Cheng, M. Lyu, S. Fan, Q. Liu, W. Zhang, Y. Zhi, C. Wang, C. Xiao, S. Wei, B. Ye and Y. Xie, *J. Am. Chem. Soc.*, 2014, **136**, 15670-15675.

S10. X. Wang, F. Li, W. Li, W. Gao, Y. Tang and R. Li, *J. Mater. Chem. A*, 2017, **5**, 17982-17989.

S11. X. Wang, L. Zhuang, Y. Jia, H. Liu, X. Yan, L. Zhang, D. Yang, Z. Zhu and X. Yao, *Angew. Chem. Int. Ed.*, 2018, **57**, 16421-16425.

S12. J. Dai, D. Zhao, W. Sun, X. Zhu, L. Ma, Z. Wu, C. Yang, Z. Cui, L. Li and S. Chen, *ACS*

Catal., 2019, **9**, 10761-10772.

S13. Y. Zhu, H. Chen, C. Hsu, T. Lin, C. Chang, S. Chang, L. Tsai and H. M. Chen, *ACS Energy Lett.*, 2019, **4**, 987-994.

S14. Y. Zhang, C. Zhang, Y. Guo, D. Liu, Y. Yu and B. Zhang, *J. Mater. Chem. A*, 2019, **7**, 2536-2540.